Polarization-Modulated Second Harmonic Generation in Collagen

Patrick Stoller,* Karen M. Reiser,† Peter M. Celliers,* and Alexander M. Rubenchik*
*Medical Technology Program, Lawrence Livermore National Laboratory, Livermore, California 94551, and †Department of Neurological Surgery, School of Medicine, University of California, Davis, California 95817 USA

ABSTRACT Collagen possesses a strong second-order nonlinear susceptibility, a nonlinear optical property characterized by second harmonic generation in the presence of intense laser beams. We present a new technique involving polarization modulation of an ultra-short pulse laser beam that can simultaneously determine collagen fiber orientation and a parameter related to the second-order nonlinear susceptibility. We demonstrate the ability to discriminate among different patterns of fibrillar orientation, as exemplified by tendon, fascia, cornea, and successive lamellar rings in an intervertebral disc. Fiber orientation can be measured as a function of depth with an axial resolution of ~10 μm. The parameter related to the second-order nonlinear susceptibility is sensitive to fiber disorganization, oblique incidence of the beam on the sample, and birefringence of the tissue. This parameter represents an aggregate measure of tissue optical properties that could potentially be used for optical imaging in vivo.

INTRODUCTION

Collagen, the most abundant structural protein in the body, is diverse in its structural and functional properties: transparent and rigid in the cornea, flexible and strong in tendons and ligaments, mineralized in bone, deformable in fascia. The specific properties of collagen (there are more than twenty genetically distinct types) in a given tissue or organ are determined not only by its primary structure but also by post-translational modifications and interactions with other connective tissue elements. The different collagens are generally categorized as either fibrillar or nonfibrillar, based on the pattern of supramolecular organization. In the present study, we focus on the fibrillar collagens, particularly type I collagen, the predominant type in the body. The fiber-forming collagens typically consist of a triple-helical macromolecule with short, nonhelical extensions at each end. Following secretion from the cell, part of the nonhelical extension at each end is cleaved off enzymatically, which triggers spontaneous self-assembly into fibrillar arrays. Fibrillar self-assembly has been studied most extensively in type I collagen; less is known about the process in the other collagen types. The basic organizational unit in the type I collagen array is the microfibril, consisting of five or six molecules. Higher levels of organization have also been defined, including subfibril, fibril, and fascicle, depending on the tissue (Beck and Brodsky, 1998; Kadler et al., 1996; Prockop and Fertala, 1998).

In several disease states, there are characteristic changes in fibrillar organization of collagen that could potentially serve as an early diagnostic marker. Early changes in collagen structure have been observed in samples analyzed using electron microscopy (Eyden and Tzaphlidou, 2001), x-ray diffraction (James et al., 1991), biochemical analysis, histological analysis, and physiological assessment. However, a major drawback of these techniques is that they are often destructive and can only be done on samples obtained through tissue biopsy. In many cases, it may not be feasible to obtain a tissue biopsy for diagnostic screening, nor may it be practical to monitor treatment with sequential biopsies. At present, there are no nondestructive, in vivo imaging techniques for detecting changes in those aspects of collagen structure and organization that define many types of pathological processes, including collagen type ratios, packing structure, fibrillar size, interaction with other matrix components, degree of fibrillar organization, and cross-linking (Reiser, 1991, 1996; Reiser et al., 1992; Knott and Bailey, 1998).

Because collagen molecules are organized naturally into structures on the scale of the wavelength of light and lack a center of inversion symmetry, they are able to generate second harmonic light, a phenomenon first observed in 1971 (Fine and Hansen). Since then, studies of second harmonic generation (SHG) in rat-tail tendon, cornea, teeth, and other tissues have been performed (Delfino, 1979; Roth and Freund, 1979, 1981; Freund et al., 1986; Altshuler et al., 1995; Georgiou et al., 2000; Theodossiou et al., 2001; Hovanessian and Lalayan, 1997; Bailey et al., 1995). The advent of ultra-short pulse lasers has allowed SHG microscopy to be performed in biological tissue without the high-intensity laser damaging the sample (Guo et al., 1996, 1997; Kim et al., 1999, 2000a,b; Campagnola et al., 2001). The works of Roth and Freund (1979, 1981) and Freund et al. (1986), and our own recent studies (Stoller et. al., 2001; Stoller et. al., in press) suggest that the polarization dependence of the second harmonic signal provides information about fiber orientation and nonlinear susceptibility not available from intensity measurements alone. The key drawback to measuring the polarization dependence is that it requires making time-consuming, repeated measurements

Submitted October 29, 2001/accepted for publication January 24, 2002.

Address reprint requests to Patrick Stoller, Medical Technology Program, Lawrence Livermore National Laboratory, L-174, P.O. Box 808, Livermore, CA 94551. Tel.: 916-734-0833; Fax: 925-424-2778; E-mail: stoller2@IInl.gov.

0006-3495/02/06/3330/13 $2.00

at a single point in the sample at different polarization angles.

In this work, we present a new SHG technique for studying collagen: imaging tissue using second harmonic light generated by a polarization-modulated ultra-short pulse laser beam. Our technique allows us to image simultaneously second harmonic intensity, collagen fiber orientation, and a parameter related to the second-order nonlinear susceptibility tensor—on microscopic scales. We use this technique to image collagen fiber orientation in tissues with very different organization: rat-tail tendon, bovine fascia, porcine cornea, human intervertebral disk, and fibrils precipitated in vitro. We also discuss changes in the second-order nonlinear susceptibility parameter as a function of tissue hydration and present preliminary findings on the effect of collagen cross-linking. The potential effects of tissue birefringence, oblique incidence of the beam on the collagen fibers, and multiple fiber orientations within the focal spot are also considered.

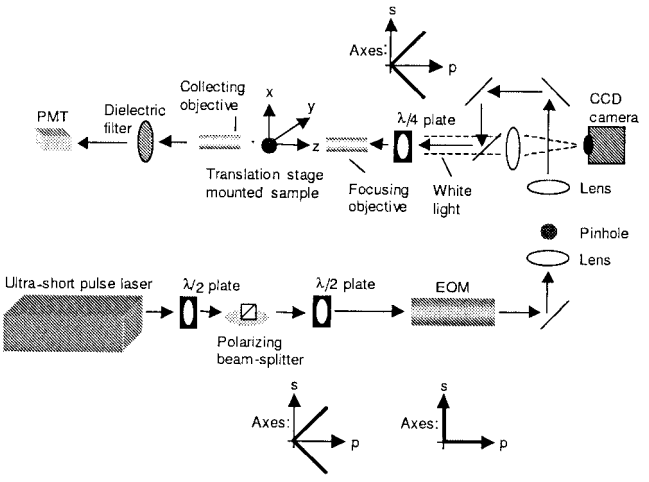

FIGURE 1 Illustration of the experimental setup.

EXPERIMENT

Optical setup

We used a Ti:Sapphire oscillator (Mira; Coherent Inc., Santa Clara, CA) to generate linearly polarized 200-fs pulses at a wavelength of 800 nm, with a maximum energy of 5 nJ, and at a repetition rate of 76 MHz. The beam passed through a half-wave plate followed by a polarizing beam-splitter; the half-wave plate was rotated to control the power incident on the sample. The p-polarized light from the beam-splitter was rotated 45° using a second half-wave plate and was then passed through an electro-optic modulator (EOM) (360-80; Conoptics, Danbury, CT) with its axes oriented at 45° to the polarization of the light. The beam was then passed through a spatial filter and beam expander, and, after reflecting off of several dielectric mirrors, through a quarter-wave plate with its axes oriented at 45° to those of the EOM. A microscope objective (infinity-corrected plano apochromat; Mitutoyo, Aurora, IL) focused the beam onto a sample mounted on an x–y–z, computer-controlled translation stage. The objective had focal length f = 1 cm, numerical aperture N.A. = 0.42, transverse resolution around 1.5 μm, and axial resolution around 10 μm. We used an objective with a relatively low numerical aperture to ensure that the polarization state of the laser beam was not substantially altered in the focus. The transmitted second harmonic signal was collected using a second objective. Several dichroic mirrors and a dielectric filter were used to reject the first harmonic and allow only the second harmonic signal to reach the photomultiplier tube (PMT) (H6780; Hamamatsu Photonics K.K., Hamamatsu City, Japan). A fiber-lamp (used while not scanning to illuminate the sample through the collecting objective), lens, and CCD camera were used to image the sample and the focal spot of the laser. The experimental setup is shown in Fig. 1.

We used the EOM and quarter-wave plate combination to rotate the polarization direction of the linearly polarized laser light. An EOM functions as a variable wave plate where the phase delay is proportional to the voltage applied across it. For linearly polarized input light, the EOM produces elliptically polarized light. The quarter-wave plate that follows the EOM converts the elliptically polarized light into linearly polarized light rotated by some angle with respect to the laser polarization direction. The degree of rotation is directly proportional to the applied voltage: from 0° for 0 V to 180° for the full-wave voltage of the EOM. The voltage across the EOM can be modulated at high frequencies; our system is limited to a bandwidth of 1 MHz.

A function generator (DS345; Stanford Research Systems, Sunnyvale, CA) provided a saw-tooth waveform at 4 kHz that was amplified to have an amplitude equal to the full-wave voltage of the modulator using a high-voltage power supply (Conoptics 302A). The polarization-modulated beam produces SHG in the sample that is modulated at the first and second harmonic of the modulation frequency (the origin of these modulations is discussed in Theory, below). After passing through a current preamplifier (SR570; Stanford Research Systems), the modulated signal from the PMT was amplified using two lock-in amplifiers (EG&G 7260; PerkinElmer, Inc., Wellesley, MA) set to detect the amplitude and phase of the SHG signal at both the first and second harmonic of the EOM modulation frequency. A Labview program was used to coordinate motion of the translation stage using a motion controller (ESP300; Newport, Irvine, CA) and Newport 850F actuators and to acquire data from the lock-in amplifiers.

Tissue source

Rat-tail tendon from 3–4-month-old Sprague-Dawley rats was frozen at −20°C until scanned. We previously had found that freezing and thawing did not affect the second harmonic signal. Individual tendon fascicles were removed from the tendon bundles under a dissecting microscope. Typical fascicles were several centimeters long, and had a diameter of only a few tenths of a millimeter.

Porcine cornea was obtained from a local abattoir. Frozen sections prepared from human intervertebral disk specimens were a kind gift of Jeff Lotz and Ellen Liebowitz of the University of California, San Francisco. Bovine fascia was obtained from bovine Achilles tendon from commercially available beef hooves.

Histological preparation

Dehydration treatment

Dehydrated rat-tail tendon was obtained by drying a rat-tail fascicle in ethanol. Baths of 30, 50, 70, 80, 90, 95, and 100% ethanol in distilled water were used in succession for thirty minutes each.

Distilled water treatment

Rat-tail tendon fascicles were also placed in distilled water; the tenuous, gel-like structure that formed after ~15 min was placed on a slide and allowed to dry. Control rat-tail tendon fascicles were maintained in 250 mM sodium phosphate, but blotted dry before scanning. Fresh bovine tendon fascia and previously refrigerated porcine cornea were placed on glass slides. The porcine cornea sample was allowed to dry before scanning; it was also scanned after being placed in distilled water, and again after it had dried.

Tissue sectioning

Frozen sections (4 μm) were prepared from some of the rat-tail tendon fascicles. Slices were obtained from the surface of the fascicle and from ~20 and 40 μm below the surface. The frozen sections were left unstained and placed on glass slides beneath a cover slip. Sections of human intervertebral disk (30 μm thick), cut parallel to the lamellar rings, were prepared in a similar manner.

In vitro fibrillogenesis from soluble collagen

Collagen fibrils were also prepared in vitro. Fibrillogenesis was initiated in neutral salt-soluble collagen and acid-soluble collagen, using techniques developed by several earlier investigators (see, for instance, Williams et al., 1978). Briefly, type I collagen from rat-tail tendon (Sigma, St. Louis, MO) was dissolved in either 0.05 M acetic acid or 20 mM sodium phosphate, pH 7.4. Solutions were clarified in a microfuge at 10,000 × g before use. Fibrils were precipitated from the acid-soluble collagen by adding 0.5 M NaOH until the pH was 8. The collagen in the sodium phosphate was kept at 4°C until fibrillogenesis was thermally initiated by increasing the temperature to 38°C in an oven. Precipitated fibrils were collected on a glass slide and allowed to air dry. In some cases, the precipitated fibrils were allowed to remain in solution for up to one week to allow cross-linking to occur, as has been previously described (Gelman et al., 1979). The presence of cross-links (formed from aldehydes already present on the soluble collagen) was confirmed by observing the effects of reversing the conditions. Collagen fibrils that had been precipitated the same day readily returned to solution if conditions were returned to the initial state. Collagen fibrils that had incubated for a week remained in their fibrillar state. A slurry of type I collagen in 0.5 M acetic acid (10 mg/mL) was lyophilized in a petri dish.

THEORY

SHG in collagen fibers

An analytical model for SHG in collagen fibers, based on the assumption of cylindrical symmetry, has been developed and extensively discussed previously (Roth and Freund, 1979, 1981; Freund et al., 1986; Stoller et. al., 2001; Stoller et al., in press). We present only a brief summary of the derivation. It is important to note that we are interested primarily in calculating the dependence of the second harmonic intensity on the polarization angle of the input beam. For any material with cylindrical symmetry (C_∞ symmetry), the most general vector expression for the second-order nonlinear polarization is

$$\vec{P} = a\hat{s}(\hat{s}\cdot\vec{E}_1)^2 + b\hat{s}(\vec{E}_1\cdot\vec{E}_1) + c\vec{E}_1(\hat{s}\cdot\vec{E}_1), \qquad (1)$$

where $\hat{s}$ represents the unit vector along the symmetry (fiber) axis, $\vec{E}_1$ is the input electric field, and a, b, and c are coefficients related to the second-order nonlinear susceptibility tensor of the material. The nonlinear susceptibility tensor is given by

$$\chi^{(2)}_{ijk} = as_i s_j s_k + bs_i\delta_{jk} + (c/2)(s_j\delta_{ik} + s_k\delta_{ij}). \qquad (2)$$

Under the assumption of Kleinman symmetry, $b = c/2$. Kleinman symmetry means that all of the elements in the nonlinear susceptibility tensor that are connected by permutation of indices are equal (see, for instance, Boyd, 1992). The assumption of Kleinman symmetry is valid because the second harmonic wavelength (400 nm) is far from the wavelength of the first electronic transition in collagen (~310 nm). Thus, we can write

$$\vec{P} = a\hat{s}(\hat{s}\cdot\vec{E}_1)^2 + b\hat{s}(\vec{E}_1\cdot\vec{E}_1) + 2b\vec{E}_1(\hat{s}\cdot\vec{E}_1). \qquad (3)$$

We further assume a Gaussian input beam, make the paraxial approximation (the interaction length is much larger than

the wavelength), and assume the laser beam is normally incident on the sample. Under these assumptions, the input laser and generated second harmonic polarization is confined to the plane normal to the laser propagation direction $\hat{k}$. Given the nonlinear polarization, $\vec{P}$, we can write down expressions for the second harmonic field $E_{2\|}$ generated along the fiber axis ($\hat{s}$) and the second harmonic field $E_{2\perp}$ generated along the normal to that axis ($\hat{s} \times \hat{k}$),

$$E_{2\|}(\vec{r}, t) = A_{2\|}(z)\hat{s}\,\frac{\exp\{i(k_2 z - \omega_2 t) - r^2/w_o^2\,[1 + i(z/z_R)]\}}{1 + i(z/z_R)},$$

$$E_{2\perp}(\vec{r}, t) = A_{2\perp}(z)(\hat{s} \times \hat{k}) \times \frac{\exp\{i(k_2 z - \omega_2 t) - r^2/w_o^2\,[1 + i(z/z_R)]\}}{1 + i(z/z_R)}, \quad (4)$$

where $A_{2\|}$ and $A_{2\perp}$ are given respectively, by the differential equations,

$$2ik_2\frac{\partial A_{2\|}}{\partial z} = -\mu\omega_2^2(\vec{P}\cdot\hat{s})\,\frac{e^{i\Delta kz}}{1 + i(z/z_R)},$$

$$2ik_2\frac{\partial A_{2\perp}}{\partial z} = -\mu\omega_2^2(\vec{P}\cdot(\hat{s} \times \hat{k}))\,\frac{e^{i\Delta kz}}{1 + i(z/z_R)}. \quad (5)$$

Here, ω_2 and k_2 are the second harmonic frequency and wave number, respectively; r and z are the radial and axial position, respectively; w_o and z_R are the focused beam waist and Rayleigh range, respectively; $\Delta k = 2k_1 - k_2$ (k_1 is the wave number at the laser frequency and k_2 the wave number at the second harmonic); and μ is the magnetic permeability. Refer to, for instance, Boyd (1992) for a detailed derivation of these expressions from Maxwell's equations. Neglecting the effect of linear birefringence (Δk is taken to be independent of the polarization direction), the polarization dependence of the second harmonic intensity (proportional to the square of the electric field) is contained entirely in the terms $\vec{P}\cdot\hat{s}$ and $\vec{P}\cdot(\hat{s}\times\hat{k})$. Thus, we can write

$$I_{SHG} \propto (\vec{P}\cdot\hat{s})^2 + (\vec{P}\cdot(\hat{s} \times \hat{k}))^2. \quad (6)$$

Polarization modulation technique

We can now apply the model discussed above to understanding our polarization modulation technique and how it can be used to obtain information about fiber orientation and nonlinear susceptibility. To simplify the discussion, we choose a coordinate system where the laser beam is incident along the z axis and polarized at an angle α with respect to the x axis. The fiber is located in the x–y plane; we let it be oriented at an angle ϕ from the y-axis. This geometry is shown in Fig. 2. Using this geometry, we can obtain an expression from Eq. 3 and Eq. 6 for the second harmonic intensity as a function of α and ϕ,

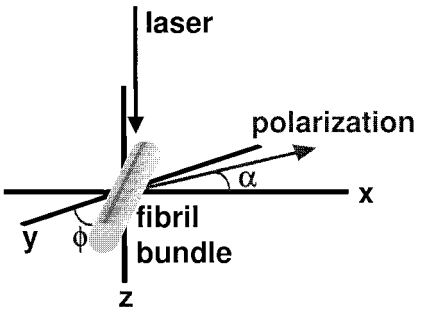

FIGURE 2 Sketch of the fiber orientation and laser beam propagation direction and orientation.

$$I_{SHG} \propto \tfrac{1}{8}(3 + 20\gamma + 40\gamma^2) - \tfrac{1}{2}(1 + 6\gamma + 8\gamma^2)\mathrm{Cos}(2\alpha + 2\phi) + \tfrac{1}{8}(1 + 4\gamma)\mathrm{Cos}(4\alpha + 4\phi). \quad (7)$$

Here we define $\gamma = b/a$; unlike a and b, γ can be determined without making any absolute intensity measurements. γ is a fundamental parameter of the second-order nonlinear susceptibility tensor—it is the ratio of the tensor's two independent elements.

To efficiently measure this fundamental parameter, the linear polarization of the laser beam is continuously rotated by driving the EOM with a saw-tooth pattern at frequency, Ω (see Fig. 3), so that $\alpha = \Omega\pi t$. Thus, we can rewrite Eq. 7 as

$$I_{SHG} \propto \tfrac{1}{8}(3 + 20\gamma + 40\gamma^2) - \tfrac{1}{2}(1 + 6\gamma + 8\gamma^2)\mathrm{Cos}(2\pi\Omega t + 2\phi) + \tfrac{1}{8}(1 + 4\gamma)\mathrm{Cos}(4\pi\Omega t + 4\phi). \quad (8)$$

It is apparent from this equation that signal can be measured at both the first modulation harmonic and second modulation harmonic (FMH and SMH) of the frequency applied to the EOM. A lock-in amplifier is capable of measuring both the amplitude and phase of a signal at a reference frequency and at harmonics of the reference frequency. The signal at the FMH is proportional to

$$I_{FMH} \propto -\tfrac{1}{2}(1 + 6\gamma + 8\gamma^2), \quad (9)$$

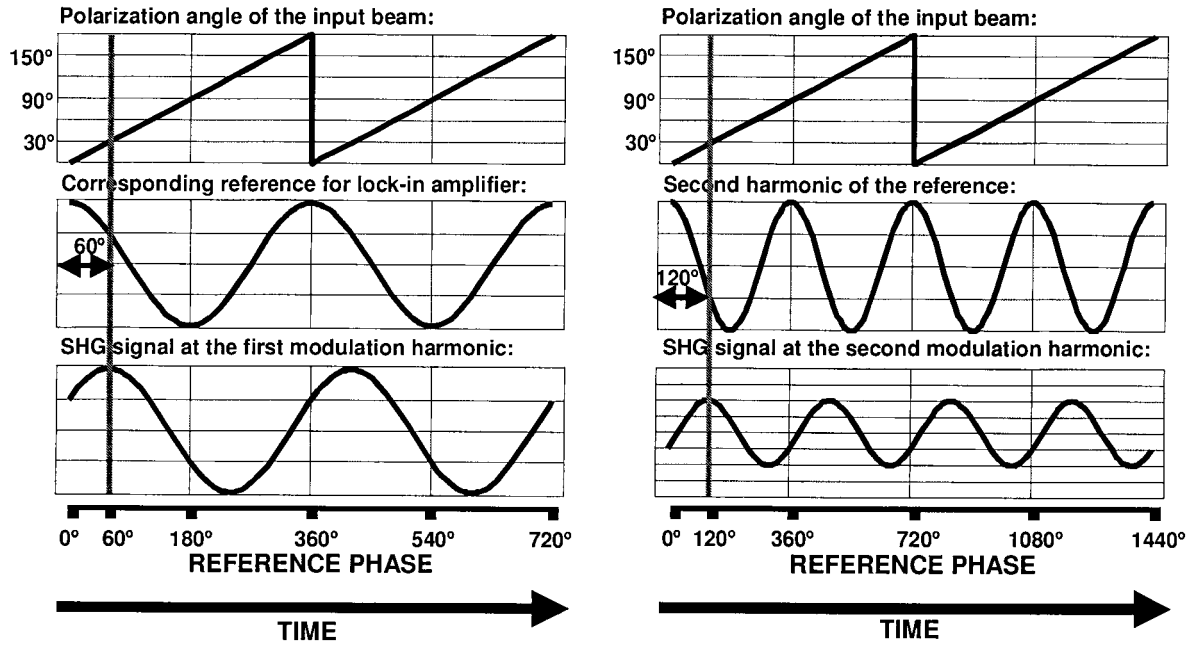

FIGURE 3 Sketch of the technique we use to obtain fiber orientation information using polarization-modulation of the input laser beam. For convenience, we assume a fiber oriented at an angle of 30° from the y axis. We assume that $R = 0.5$. All plots have a common time axis. The case for the FMH of the signal is shown on the left and the case for the SMH of the signal is shown on the right. The vertical line is drawn through the curves at the point in time when the input beam is polarized in the direction of the fiber; the SHG signal peaks at this time. From the plots, it is evident that twice the orientation angle is equal to the phase shift of the signal at the FMH, and four times the orientation angle is equal to the phase shift of the signal at the SMH.

whereas the signal at the SMH is proportional to

$$I_{\mathrm{SMH}} \propto \tfrac{1}{8}(1 + 4\gamma). \tag{10}$$

The ratio R of the amplitude of the signal at the FMH and SMH can thus be written as

$$R = -\tfrac{1}{4} + 8\gamma. \tag{11}$$

Eq. 11 shows that γ can be rapidly measured using amplitude measurements from two lock-in amplifiers. Furthermore, the intensity of the second harmonic signal at the FMH and SMH is independent of the fiber orientation. All of the information about orientation is conveyed by the phase of the FMH and SMH signal. A lock-in amplifier measuring the phase at the FMH will measure 2ϕ, and a lock-in amplifier measuring the phase at the SMH will measure 4ϕ. Thus, half of the phase of the FMH signal is equal to the fiber orientation, ϕ. The phase of the SMH signal provides redundant information about the fiber orientation, but the phase difference between twice the FMH phase and the SMH phase (0° or 180°) gives the sign of the ratio R. Refer to Fig. 3 for a diagram illustrating the use of polarization modulation and phase-sensitive detection to determine fiber orientation.

Eq. 11 indicates a direct relationship between the observable R and a tissue optical property γ. However, several assumptions are required for this relationship to hold. First, we have assumed that the beam is normally incident on the rat-tail tendon fascicle and that all of the fibers in the fascicle are perfectly aligned. Second, we have assumed that the effect of linear birefringence in the tissue on the polarization state of the input laser light can be neglected. For a given value of γ, what is the effect of relaxing each of these assumptions on the observable R? Calculating the effect of non-normal incidence on the fiber is straightforward. The generated second-order polarization is simply split into a component along the propagation direction and a component normal to it; we assume that the component in the propagation direction does not contribute to a significant degree; this is strictly true only in the plane-wave approximation, but is a reasonably good approximation even for a focused beam (Huse et al., 2001). Let ψ be the angle between the laser propagation direction and the normal to the fiber. The resulting change predicted in the absolute value of the measured ratio R as a function of ψ is plotted in Fig. 4 for a typical value of $\gamma = -0.7$ (based on Stoller et al., in press). This effect becomes less important as the absolute value of γ increases. A similarly simple calculation can be performed to take into account the presence of multiple fibers oriented at different angles within the focal spot of the laser beam. For illustration, we show, in Fig. 5, the results for the simple case of two fibers oriented at varying angles with respect to each other.

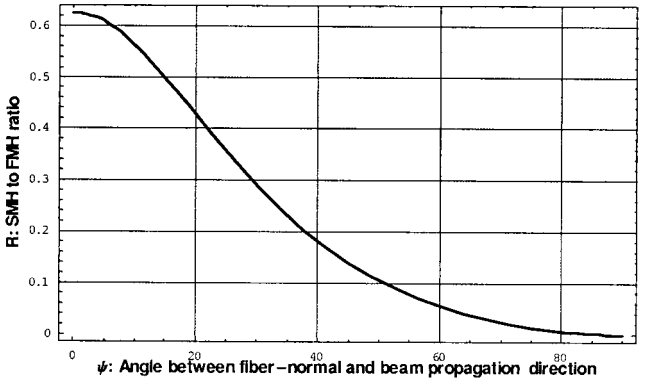

FIGURE 4 Plot of R versus the angle ψ between the laser propagation direction and the normal to the fibers, for the case of $\gamma = -0.7$.

Adding the effect of birefringence to our calculation is more complicated. Collagen is birefringent because the index of refraction for light polarized along the fiber axis is higher than that for light polarized perpendicular to the axis. An arbitrary linearly polarized beam will transform into an elliptically polarized beam as it propagates into a birefringent medium. The change in polarization state must be incorporated into the equations that propagate the light through the nonlinear medium (Eqs. 4 and 5). For simplicity, we assume a coordinate system where the collagen fiber is oriented along the y axis. We must calculate both the component of the second harmonic signal $I_{\mathrm{shg_x}}$ polarized perpendicular to the fiber and the component $I_{\mathrm{shg_y}}$ polarized parallel to the fiber. The nonlinear susceptibility tensor allows three possibilities: 1) a component of the input beam along the fiber and a component normal to it can produce second harmonic light normal to the fiber, 2) a component of the input beam normal to the fiber can produce second harmonic light parallel to the fiber, and 3) a component of the input beam parallel to the fiber can produce second harmonic light parallel to the fiber. If we integrate Eq. 5 for

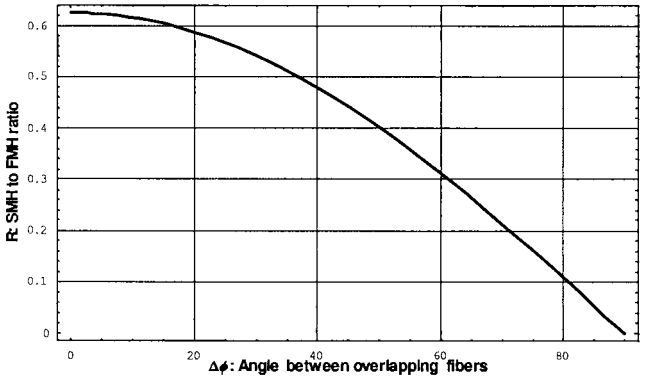

FIGURE 5 Plot of R versus $\Delta\phi$ (for $\gamma = -0.7$), where $\Delta\phi$ is the angle between two overlapping fibers, both located in the plane normal to the propagation direction.

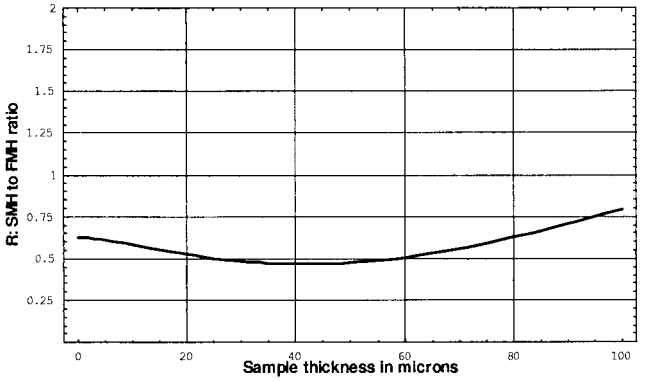

FIGURE 6 The effect of birefringence on R. Plot of R versus thickness of tissue (for $\gamma = -0.7$). The plots are shown for dispersion $n_{2\omega} - n_{\omega} = 0$ and birefringence $n_{\parallel} - n_{\perp} = 0.003$. The Rayleigh range has been taken to be 5 μm, and the beam was focused at the center of the sample.

each of these cases (taking into account the different wave vectors for different polarization directions), we have

$$I_{\mathrm{SHG_x}} \propto \left| 2bA_{1x}A_{1y} \times \int_{-L}^{-L+S} \frac{\mathrm{Exp}[i(k_{1x} + k_{1y} - k_{2x})\,(z+L)}{1 + i(z/z_R)}\,dz \right|^2, \tag{13}$$

$$I_{\mathrm{SHG_y}} \propto \left| bA_{1x}^2 \int_{-L}^{-L+S} \frac{\mathrm{Exp}[i(2k_{1x} - k_{2y})\,(z+L)}{1 + i(z/z_R)}\,dz + (a+3b)A_{1y}^2 \int_{-L}^{-L+S} \frac{\mathrm{Exp}[i(2k_{1y} - k_{2y})\,(z+L)]}{1 + i(z/z_R)}\,dz \right|^2. \tag{14}$$

In these expressions, L represents the distance from the front surface to the focal point, and S refers to the sample thickness. A_{1x} and A_{1y} depend on the input polarization angle α, and the Fourier components of $I_{\mathrm{shg}} = I_{\mathrm{shgx}} + I_{\mathrm{shg_y}}$ are readily calculated to obtain R. The change in the measured ratio due to birefringence in a structure with uniform collagen orientation throughout depends on several parameters: the size of the focal volume, the depth of the focus in the material, and the degree of birefringence (which is sensitive to the index of refraction of the surrounding medium). Figure 6 shows plots of the absolute value of R versus thickness in a sample with the beam focused at the center (we again take $\gamma = -0.7$). Measurements of birefringence in collagen indicate that $n_{\parallel} - n_{\perp} \sim 0.003$ (Bolin et al., 1989; Maitland, 1995; Poh, 1996); for simplicity, we neglect dispersion and use this value in calculating the plots

shown in Fig. 6. The effect of birefringence will be smaller in tissues (such as cornea or intravertebral disk) where fibers are not aligned along one direction consistently throughout the depth of the tissue.

Birefringence, oblique incidence, and fiber disorganization all affect the value of R measured for a given value of γ. Thus, except in the case of thin sections with fibers organized on the scale of the beam waist and oriented in the plane normal to the beam, R is related only indirectly to the nonlinear susceptibility tensor.

RESULTS

Images of fibrillar orientation in tissue

We selected tissues with increasingly complex fiber orientation patterns for study. We wanted to determine whether our scanning technique could clearly distinguish among these patterns; in addition, we wanted to see whether fibrillar organization determined by SHG analysis correlated with morphological information obtained by conventional methodologies such as electron microscopy (Eyden and Tzaphlidou, 2001). We first chose a tissue, rat-tail tendon fascicle, in which the fibril bundles lie parallel to each other and the orientation is very homogeneous throughout. Figure 7 shows a scan across a section of rat-tail tendon fascicle. The section scanned lies in the plane perpendicular to the laser beam (the x–y plane; refer back to Fig. 2). The line segments in the figure are oriented along the local fiber direction.

We next wanted to observe the second harmonic orientation image when fibrillar orientation changed in a controlled way. We performed a two-dimensional scan in a model of orientation change consisting of two overlaid fascicles at right angles to each other. We performed a depth scan in which the beam traveled from the top of the upper fascicle down to the bottom of the lower fascicle. In other words, we obtain data in the x–z plane through two fascicles lying parallel to the x axis and y axis, respectively. The orientation data from this model are shown in Fig. 8. The transition from one orientation to the other is abrupt, occurring within the 10-μm axial optical resolution of the microscope objective used. In this case, the y-scan axis refers to an arbitrary direction in the plane of the rat-tail tendon fascicle, normal to be the beam. The z-scan axis refers to the direction along which the laser propagates. Increasing z coordinate corresponds to increasing depth in the tissue ($z = 0$ has been chosen to approximate the surface). Note that the orientation line segments in this figure still lie in the x–y plane and not in the x–z plane.

We next analyzed a tissue characterized by regular changes in fibrillar orientation in the lamellar rings of intervertebral disks. Fibrillar orientation alternates by ~60° (relative to the vertical axis of the spinal cord) in successive lamellar rings. Figure 9 *A* shows a visible light micrograph

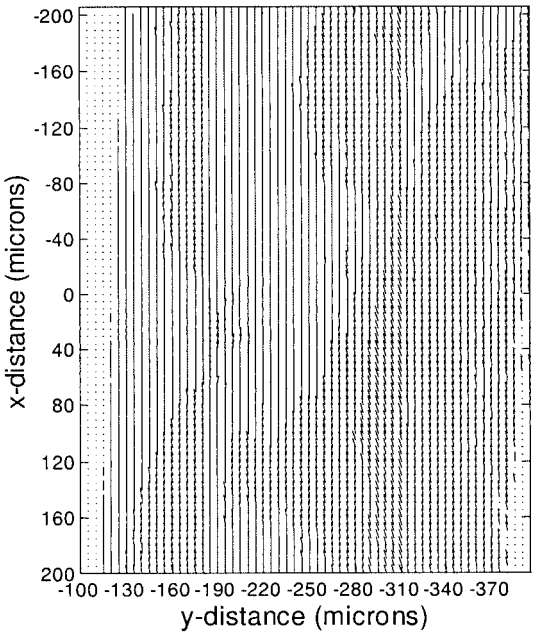

FIGURE 7 Orientation image of an x–y section of rat-tail tendon (fascicle aligned in the plane normal to the laser beam propagation direction). The orientation line segments indicate the very uniform fiber orientation. All segments are drawn to the same length.

(obtained from the CCD camera) of a 30-μm-thick frozen section of intervertebral disk. Figure 9 *B* gives a plot of the orientation data in approximately the same region as shown in the micrograph. Figure 9 *C* is a histogram of fiber orientation, indicating that the difference in orientation between the two regions is ~60°.

We chose to image cornea because of its unique, interwoven collagen structure (Kay, 1988). Figure 10 illustrates fiber orientation in a 0.5 × 0.5-mm region near the top surface of a porcine cornea. We observe a pattern of many discrete regions (with a length scale of ~50 μm) of parallel fibers. We saw a similar pattern of discrete regions containing parallel fibers in bovine tendon fascia (Fig. 11 *A*). It is striking that these regions were ~1/25 the area of those in cornea (Fig. 11 *B*).

Images of fibrillar orientation in lyophilized fibrils

We also obtained orientation images in lyophilized fibrils precipitated from type I collagen to have more direct control over specific structural features that may play a role in SHG. Figure 12 *A* shows fiber orientation in lyophilized Type I collagen—there is very little organization on a scale larger than our scan resolution of 5 μm. Interestingly, the collagen at the intersection between the wall and the bottom of the dish appeared to be more organized to the naked eye. Figure 12 *B* shows fiber orientation in this region, showing marked homogeneity of orientation.

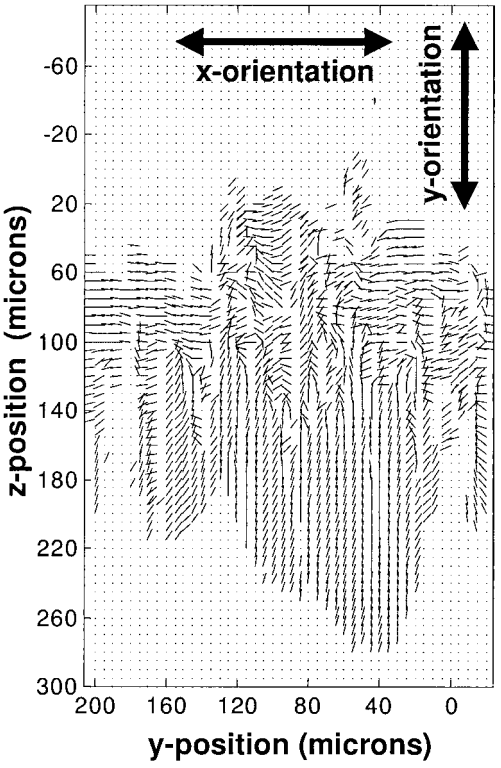

FIGURE 8 Orientation image of a y–z section of two overlapping rat-tail tendon fascicles (fascicles aligned in the plane normal to the laser beam propagation direction, at an angle of ~90° to each other). The samples have been slightly compressed between glass slides. The point $z = 0$ refers approximately to the surface of the top fascicle; depth in the fascicles increases with increasingly positive z. Note that the orientation lines in the image are not in the y–z plane; they are in the x–y plane, normal to the beam.

Measurement of *R*

The same scans that yielded the orientation data also provide information about the second-order nonlinear susceptibility of the material. Values of R measured in frozen sections of rat-tail tendon, where fiber overlap, birefringence, and oblique incidence are not significant, are consistently around $R = 1.0$, with a standard deviation of ~0.4. The effect of fiber disorganization on R is readily apparent in thicker tissues where birefringence, oblique incidence, and fiber overlap can influence the measurement in an unpredictable manner. The average measured value of R varies considerably from fascicle to fascicle, even when tissue from the same rat was studied; mean values between +0.3 and +0.9 have been measured. In some of the rat-tail tendon frozen sections, the sectioning technique led to folding or crumpling of the tissue rather than producing uniform sections. Unlike in the uniform frozen sections discussed above, fiber overlap and oblique incidence of the beam on the collagen fibers can have a significant effect on R in these sections. The disorder is

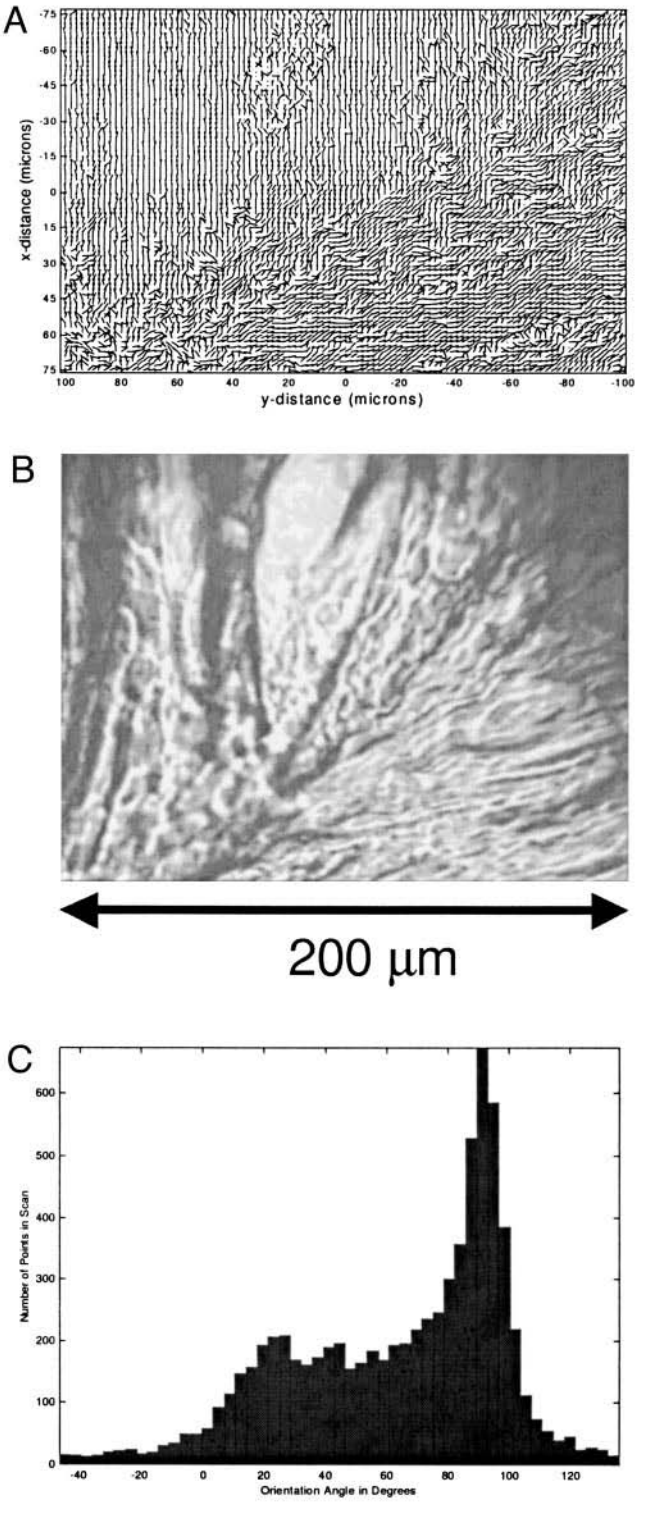

FIGURE 9 (*A*) Visible light micrograph of a small region of an x–y section of intervertebral disk showing two different regions of fiber orientation. (*B*) Orientation image of approximately the same region. (*C*) Histogram showing the frequency of fiber orientation in the intervertebral disk scan shown in (*B*). Note that there are two peaks in the distribution, separated by ~60°.

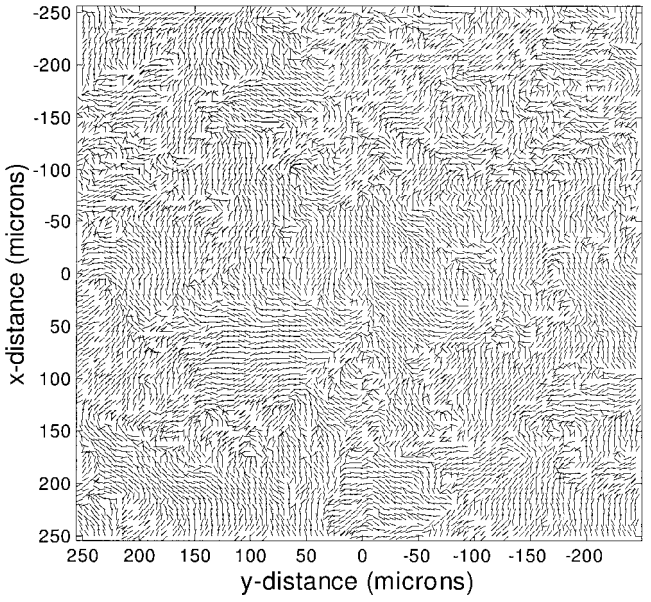

FIGURE 10 Orientation image of an x–y region of porcine cornea. The surface of the cornea was oriented normal to the laser propagation direction.

readily apparent in the white-light images (for example, Fig. 13 *A*) of the tissue sections. An SHG scan of the approximate region shown in the micrograph leads to the fiber orientation image shown in Fig. 13 *B* and the *R*-image shown in Fig. 13 *C*. Clearly, *R* is lower in regions where the fibers are overlapping or are not oriented in the plane of the slice. These results confirm the predictions of our theory (refer back to Fig. 4 and 5).

Properties that affect *R*

Hydration

The degree of tissue hydration appears to be correlated with *R*. We observed a change in the ratio when rat-tail tendon samples were removed from phosphate-buffered saline and dried in baths of increasingly concentrated alcohol. The mean ratio $R = +0.89$ with a standard deviation of 0.51 was observed in a sample moistened in 250 mM $NaPO_4$ and dried in air for ~10 min, whereas a ratio $R = +0.05$ with a standard deviation of 0.19 was observed in the alcohol-dried sample. Samples dried to lesser degree in alcohol (dried only through the 70% alcohol step, as discussed in Experiment, above) showed intermediate values of R. These changes were not associated with any significant change in the intensity of the signal.

Fibrillar organization

We measured *R* in samples of lyophilized pure Type I collagen. A value of $R = +0.01 \pm 0.17$ was observed,

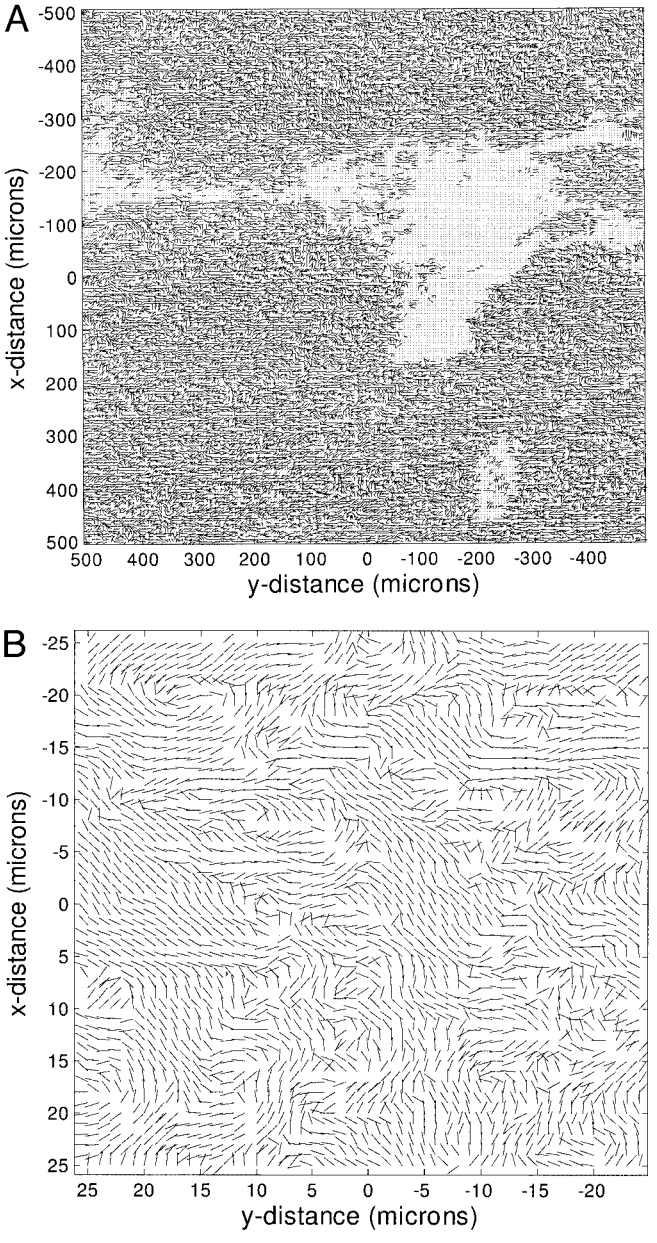

FIGURE 11 (*A*) Orientation image of an x–y region of bovine tendon fascia, with a spatial resolution of 5 μm. (*B*) Orientation image of the region between (−25, −25) and (25, 25) in (*A*), but measured with a spatial resolution of 1 μm. Note the similarity between this image and the one in Figure 10, aside from a tenfold change in scale.

significantly lower than the value observed in native rat-tail tendon. The intensity of the SHG signal was one to two orders of magnitude below that observed in rat-tail tendon. We initially thought that low values of *R* could be associated with the lack of a discernible pattern of fibrillar orientation (refer back to Fig. 12 *A*). However, we obtained similar *R* measurements in the region where a highly organized, parallel array of collagen fibrils formed (Fig. 12 *B*). For the organized precipitated fibrils, $R = +0.03 \pm 0.17$,

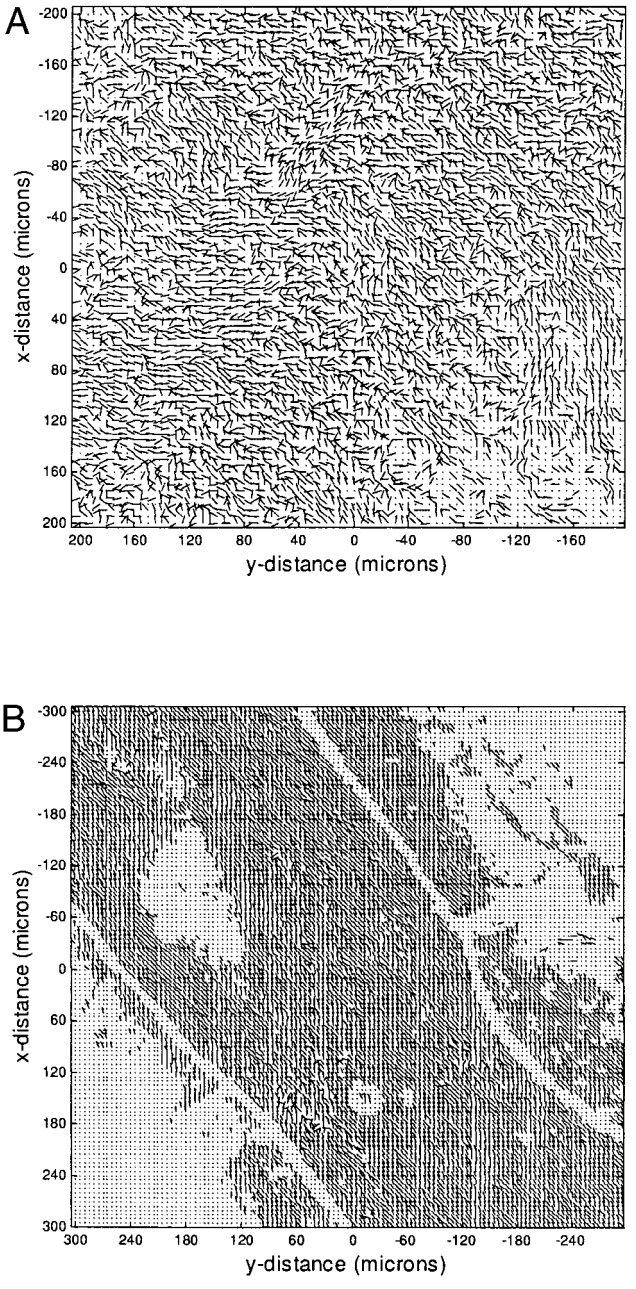

FIGURE 12 (*A*) Orientation image of lyophilized collagen fibers. The SHG scan was performed near the center of the petri dish in a region of typically random fiber orientation. (*B*) Orientation image of lyophilized collagen fibers. The SHG scan was performed near the edge of the petri dish.

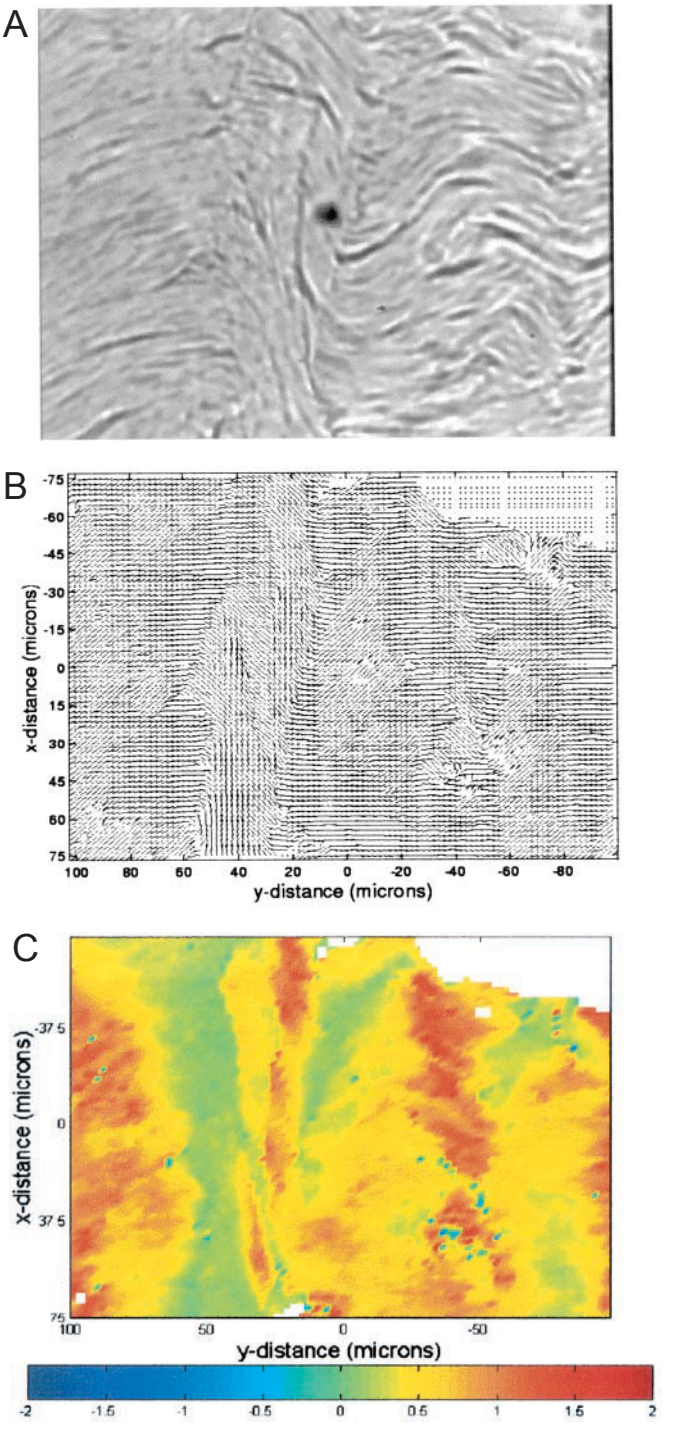

FIGURE 13 (*A*) Visible light image of a small region of a frozen section of rat-tail tendon. The image shows how parts of the section have been folded and twisted. (*B*) Orientation image of the approximate region shown in (*A*). (*C*) Measurement of R in the same region as (*B*), plotted as a function of position in the sample.

but the intensity is comparable to that measured in rat-tail tendon.

Conditions of fibrillogenesis

We also looked at the effect of the conditions of fibrillogenesis. Similar results were observed in collagen fibers precipitated from both acid-soluble and neutral salt-soluble type I collagen. The signal intensity (FMH) was two to three orders of magnitude below that observed in native rat-tail

tendon. The SMH intensity was too close to the noise threshold to allow accurate determination of R (but R was clearly $<\sim 0.2$). We initially suspected that the dramatically decreased values of R could be attributed to lysyl-oxidase-mediated cross-linking between collagen molecules. We compared data from fibrils precipitated one hour before scanning with fibrils precipitated one week earlier. As noted in Experiment, a one-week incubation is sufficient for cross-link formation. The crosslinked collagen had the same ratio as the uncross-linked collagen.

Suprafibrillar organization

We decided to disrupt fascicular structure in step-wise fashion by inducing lyotropic swelling within the fascicle. This phenomenon involves no denaturation or disruption of the fibril itself; rather, it loosens the bonds between adjacent fibrils by causing them to swell laterally (Gustavson, 1956). In the case of fascicles, the swelling fibrillar bundles will first lose their crimp angle and eventually burst the enclosing fascial sheath. Fascicles placed briefly in water (1 min) will, upon drying, return to a grossly normal appearance, including the presence of crimp angle. However, once the fascial sheath has burst, the fascicle does not regain a normal appearance after dehydration. The individual fibrillar bundles remain dispersed in an amorphous gel-like structure. In fascicles in which swelling was induced up to the point of loss of crimp angle (1 min), and which were subsequently dehydrated, we observed little change in R and in signal intensity. In contrast, in dehydrated samples that had been subjected to water until the fascial sheath burst, R and signal intensity were both significantly lower.

To determine that the water-induced disruption of suprafibrillar organization rather than the water per se caused the changes in R, we examined lyotropic swelling in a very different tissue. Collagen in cornea imbibes water to the same degree as fascicular collagen. However, there is no permanent structural alteration resulting from the fibrillar swelling. We observed that the signal intensity and R in both hydrated and dehydrated cornea were not significantly different.

DISCUSSION

Our images of second harmonic signal—both those of the fiber orientation (from the phase information) and those of the ratio of the two modulation harmonics, R—demonstrate that these parameters can be measured at high resolution in tissue. Because SHG depends on the square of the input laser intensity, the effect is localized to the focal volume of the microscope objective ($\sim 1\ \mu$m in the transverse direction and $\sim 10\ \mu$m in the axial direction). Orientation information is not limited to surface regions that might be accessible to other techniques for determining orientation. Techniques such as polarization-sensitive optical coherence tomography are also able to obtain information related to collagen fiber orientation as a function of depth (Tadrous, 2000). However, they yield data that depends on the depth through which the light propagates; to the best of our knowledge, direct information about the orientation is not available from this technique.

Using thin, highly organized sections of rat-tail tendon fascicle, we are able to determine from the measured values of R that γ is between -0.6 and -0.7 for this type of collagen. In less ideal samples, our results show that there are many other things that can affect the measured value of R, besides the second-order nonlinear susceptibility tensor itself. For instance, the value of R (for values of γ relevant to collagen fibers) is largest in those fibers oriented normal to the laser beam propagation direction and decreases progressively for fibers oriented with some component along this direction. Although this might provide useful in determining orientation in the direction along the laser beam in some situations, it makes measuring γ, the actual ratio of the elements in the second-order nonlinear susceptibility tensor, more difficult. Fibers located within the Rayleigh range ($\sim 10\ \mu$m) of each other can add coherently to the second harmonic signal; if these fibers are oriented at different angles, this may also lead to a reduction in R. The birefringence of the tissue, especially in highly organized structures such as rat-tail tendon where all of the fibers are oriented parallel to each other, can also change the value of R measured.

Under many of the conditions used in our experiments, we observed a decrease in R to very low levels. What does a low value of R mean physically? Assuming that the effects of birefringence, oblique incidence, and overlapping fibers are small (true for the thin, highly oriented sample of lyophilized collagen, for example) as R approaches zero, γ approaches negative infinity. Because $\gamma = b/a$ is the ratio of the two independent elements of the second-order nonlinear susceptibility tensor, this implies that a goes to zero as R goes to zero. In the other extreme, for a large ratio, γ approaches -0.5 and a approaches $-2b$. If we take the simple case of a beam polarized at 45° to the fiber axis, $a = 0$ implies that (see Eq. 13 and 14) the ratio between SHG intensity parallel to the fiber and SHG intensity perpendicular to the fiber is 4:1. In contrast, $a = -2b$ implies that this ratio is 1:1. Therefore, as R decreases, the SHG signal produced by an input beam polarized at 45° to the fiber axis becomes increasingly polarized along the fiber axis. We suspect, for instance, that, in tissue dried in alcohol, the reduction of highly polar water molecules reduces the nonlinear polarizability normal to the fiber direction and thus leads to a low value of R.

Many of the experiments were aimed at identifying which features of the structure and organization of fibrillar collagen play the largest role in determining the signal intensity and R. Based on the studies of alcohol-dried rat-tail tendon fascicles we suspect that hydration level significantly low-

ers R, but not the signal intensity. We also examined collagen fibrils precipitated in vitro to avoid possible confounding effects of other connective tissue elements. Cross-linking does not appear to affect either R or the signal intensity. Our studies suggest that fibrillar organization plays an important role in determining the properties of SHG in collagen. In rat-tail tendon, where R is of order 0.5, disrupting the fibrillar orientation (through lyotropic swelling) results in a decrease in R and in the signal intensity. Similarly, in lyophilized collagen, the signal intensity is significantly lower in unorganized regions than in regions where fibrils appear grossly in parallel arrays. However, increased second harmonic signal intensity is not associated with an increase in R. Furthermore, previous studies have shown that the packing structure of precipitated fibrils is the same as that of the native fibrils, manifested by the 67-nm periodicity observed in electron microscopy images (Williams et al., 1978). Therefore, we conclude that the level of organization that plays a major role in determining R is neither at the molecular nor at the fibrillar level. Our data suggest that a level of organization involving alignment within fibrillar bundles is responsible; the nature of this alignment is not known. If this alignment is disrupted in native fascicles, it appears to be irreversible.

CONCLUSION

Our technique provides a fairly robust measurement of fiber orientation, even at depths of order 100 μm in tissue. In samples prepared in optimal ways (parallel fibers in thin sections aligned in the plane normal to the beam) the observable R may be used to extract γ, the ratio of the two independent elements of the nonlinear susceptibility tensor. In the more general situation, R is influenced by birefringence, by the degree of fiber disorganization, and by non-normal incidence of the laser beam on a fiber. It can be used as an aggregate measure of tissue optical properties. Our experimental data suggests that the property with the most influence on SHG in fibrillar collagen is the degree of organization at the suprafibrillar level.

We thank Jeff Lotz and Ellen Liebowitz at the University of California, San Francisco Department of Orthopedic Surgery for providing us with frozen sections of human intervertebral disk tissue.

This work was supported by grants from the National Institutes of Health, 1 R01 AR 46885-01 and from the Center of Excellence for Laser Applications in Medicine, U.S. Department of Energy DE-FG03-98ER62576. This work was performed under the auspices of the U.S. Department of Energy at Lawrence Livermore National Laboratory under contract W-7405-ENG-48.

REFERENCES

Altshuler, G. B., N. R. Belashenkov, G. A. Martsinovski, and A. A. Solounin. 1995. Nonlinear transmission and second-harmonic generation in dentin in the field of ultrashort ND-laser pulses. *In* Advanced Laser Dentistry. G. B. Altshuler, R. J. Blankenau, and H. A. Wigdor, editors. *Proc. SPIE.* 1984:6–10.

Bailey, R. T., F. R. Cruickshank, D. Pugh, J. N. Sherwood, and S. Wilkie. 1995. Nonlinear optical behaviour of fish scales. *Ferroelectrics.* 1995: 293–299.

Beck, K., and B. Brodsky. 1998. Supercoiled protein motifs: the collagen triple-helix and the α-helical coiled coil. *J. Struct. Biol.* 122:17–29.

Bolin, F. P., L. E. Preuss, R. C. Taylor, and R. J. Ference. 1989. Refractive index of some mammalian tissues using a fiber optic cladding method. *Appl. Optics.* 28:2297–2303.

Boyd, R. W. 1992. Nonlinear Optics. Academic Press, San Diego, CA.

Campagnola, P. J., H. A. Clark, W. A. Mohler, A. Lewis, and L. M. Loew. 2001. Second-harmonic imaging microscopy of living cells. *J. Biomed. Optics.* 6:277–286.

Delfino, M. 1979. A comprehensive optical second harmonic generation study of the non-centrosymmetric character of biological structures. *J. Biol. Phys.* 6:105–117.

Eyden, B., and M. Tzaphlidou. 2001. Structural variations of collagen in normal and pathological tissues: role of electron microscopy. *Micron.* 32:287–300.

Fine, S., and W. P. Hansen. 1971. Optical second harmonic generation in biological tissues. *Appl. Optics.* 10:2350–2353.

Freund, I., M. Deutsch, and A. Sprecher. 1986. Connective tissue polarity: optical second-harmonic microscopy, crossed-beam summation, and small-angle scattering in rat-tail tendon. *Biophys. J.* 50:693–712.

Gelman, R. A., B. R. Williams, and K. A. Piez. 1979. Collagen fibril formation: evidence for a multistep process. *J. Biol. Chem.* 254: 180–186.

Georgiou, E., T. Theodossiou, V. Hovhannisyan, K. Politopoulos, G. S. Rapti, and D. Yova. 2000. Second and third optical harmonic generation in type I collagen, by nanosecond laser irradiation, over a broad spectral region. *Optics Comm.* 176:253–260.

Guo, Y., P. P. Ho, H. Savage, D. Harris, P. Sacks, S. Schantz, F. Liu, N. Zhadin, and R. R. Alfano. 1997. Second-harmonic tomography of tissue. *Optics Lett.* 22:1323–1325.

Guo, Y., P. P. Ho, A. Tirksliunas, F. Lui, R. R. Alfano. 1996. Optical harmonic generation from animal tissues by the use of ps and fs laser pulses. *Appl. Optics.* 35:6810–6813.

Gustavson, K. H. 1956. Swelling of Collagen, Donnan Effects. *In The Chemistry and Reactivity of Collagen.* Academic Press, New York. 155–170.

Hovanessian, V., and A. Lalayan. 1997. Second harmonic generation in biofiber-containing tissue. *Proc. Int. Conf. Lasers.* 96:107–109.

Huse, N., A. Schönle, S. W. Hell. 2001. Z-polarized confocal microscopy. *J. Biomed. Optics.* 6:273–276.

James, V. J., L. Delbridge, S. V. McLennan, and D. K. Yue. 1991. Use of x-ray diffraction in study of human diabetic and aging collagen. *Diabetes.* 40:391–394.

Kadler, K. E., D. F. Holmes, J. A. Trotter, and J. A. Chapman. 1996. Collagen fibril formation. *Biochem. J.* 316:1–11.

Kay, E.-D. P. 1988. Molecular anatomy of the vertebrate eye: distribution of collagen in ocular tissue. *In* Collagen: Biochemistry. Vol. 1. Marcel E. Nimni, editor. CRC Press, Boca Raton, FL. 207–224.

Kim, B.-M., J. Eichler, and L. B. Da Silva. 1999. Frequency doubling of ultrashort laser pulses in biological tissues. *Appl. Optics.* 38:7145–7150.

Kim, B.-M., J. Eichler, K. M. Reiser, A. M. Rubenchik, L. B. Da Silva. 2000a. Collagen structure and nonlinear susceptibility: effect of heat, glycation, and enzymatic cleavage on second harmonic signal intensity. *Lasers Surg. Med.* 27:329–335.

Kim, B.-M., P. Stoller, K. M. Reiser, J. Eichler, M. Yan, A. M. Rubenchik, and L. B. Da Silva. 2000b. Confocal imaging of biological tissues using second harmonic generation. *Proc. SPIE.* 3914:435–440.

Knott, L., and A. J. Bailey. 1998. Collagen cross-links in mineralizing tissues: a review of their chemistry, function and clinical relevance. *Bone.* 22:181–187.

Maitland, D. J. 1995. Dynamic measurements of tissue birefringence: theory and experiments. Ph.D. Dissertation, Northwestern University, Evanston, IL.

Poh, D. T. 1996. Examination of refractive index of human epidermis in-vitro and in-vivo. *Proc. Inter. Conf. Lasers. '96.* 118–125.

Prockop, D. J., and A. Fertala. 1998. The collagen fibril: the almost crystalline structure. *J. Struct. Biol.* 122:111–118.

Reiser, K. M. 1991. Nonenzymatic glycation of collagen in aging and diabetes. *Proc. Soc. Exper. Biol. Med.* 196:17–29.

Reiser, K. M. 1996. Extracellular matrix. *Encycl. Gerontol.* 1:519–529.

Reiser, K. M., R. J. McCormick, R. B. Rucker. 1992. Enzymatic and nonenzymatic cross-linking of collagen and elastin. *FASEB J.* 6:2439–2449.

Roth, S., and I. Freund. 1979. Second harmonic generation in collagen. *J. Chem. Physics.* 70:1637–1643.

Roth, S., and I. Freund. 1981. Optical second-harmonic scattering in rat-tail tendon. *Biopolymers.* 20:1271–1290.

Stoller, P., B.-M. Kim, A. M. Rubenchik, K. M. Reiser, L. B. Da Silva. 2001. Measurement of the second order nonlinear susceptibility of collagen using polarization modulation and phase-sensitive detection. Commercial and Biomedical Applications of Ultrashort-pulse Lasers. *Proc. SPIE.* 4276:11–16.

Stoller, P., B.-M. Kim, K. M. Reiser, A. M. Rubenchik, and L. B. Da Silva. Polarization dependent optical second harmonic imaging of rat-tail tendon. *J. Biomed. Optics.* In press.

Tadrous, P. J. 2000. Methods for imaging the structure and function of living tissues and cells: I. Optical coherence tomography. *J. Pathol.* 191:115–119.

Theodossiou, T., E. Georgiou, V. Hovhannisyan, and D. Yova. 2001. Visual observation of infrared laser speckle patterns at half their fundamental wavelength. *Lasers Surg. Med.* 16:34–39.

Williams, B. R., R. A. Gelman, D. C. Poppke, and K. A. Piez. 1978. Collagen fibril formation: optimal in vitro conditions and preliminary kinetic results. *J. Biol. Chem.* 253:6578–6585.